

# Effects of large-scale non-axisymmetric perturbations in the mean-field solar dynamo.

V.V. Pipin<sup>1,2,3</sup> and A.G. Kosovichev<sup>3,4,5</sup>

<sup>1</sup>Institute of Solar-Terrestrial Physics, Russian Academy of Sciences,

<sup>2</sup> Institute of Geophysics and Planetary Physics, UCLA, Los Angeles, CA 90065, USA

<sup>3</sup>Hansen Experimental Physics Laboratory, Stanford University, Stanford, CA 94305, USA

<sup>4</sup>Big Bear Solar Observatory, New Jersey Institute of Technology, Big Bear, CA 92314, USA

<sup>5</sup>Crimean Astrophysical Observatory, Nauchny, Crimea, 98409, Ukraine

Received \_\_\_\_\_; accepted \_\_\_\_\_

## Abstract

We explore a response of the non-linear non-axisymmetric mean-field solar dynamo model to the shallow non-axisymmetric perturbations with the strength of 1G. The amplitude of the non-axisymmetric field depends on the initial condition, helicity conservation, the depth of perturbation. It is found that perturbation which is anchored at the  $0.9R$  have a profound effect and it produce the transient magnetic cycle of the axisymmetric magnetic field if it is initiated at the growing phase of the cycle. The non-symmetric about equator perturbation results the hemispheric asymmetry of the magnetic activity. The evolution of the axisymmetric and non-axisymmetric field depends on how well the magnetic helicity is conserved. In the range of  $R_m = 10^{4-6}$  the evolution returns to the normal course in the next cycle and the non-axisymmetric field is generated due to non-linear  $\alpha$ -effect and the magnetic buoyancy. In the stationary state of evolution the large-scale magnetic field demonstrate, the phenomena of the “active longitude” and the cyclic  $180^\circ$  flip-flop of the orientation of the large-scale magnetic field. We do not use any assumptions about the non-axisymmetric distribution of the turbulent parameters. The flip-flop effect is demonstrated for the first time in the solar type dynamo model. This effect disappears in the model which includes meridional circulation. The rotation periods of the equatorial dipole evolves from the period of 25.2 days during the relaxation epoch to the period of 27 days at the stationary state of evolution.

## 1. Introduction

In mean-field dynamo models it is commonly assumed that the magnetic activity of the Sun is approximately axisymmetric on large spatial (size of the Sun) and temporal (the period of solar cycle) scales. These models provide quantitative self-consistent description of the 22-year solar magnetic cycles, and allow us to investigate the basic mechanisms of the solar dynamo. However, deviations from the axisymmetry are rather strong at any particular moment of observations. Intermittent patterns of magnetic fields on the solar surface are formed because the magnetic field emerges in the form of localized active regions. Such phenomena make a significant contribution to the large-scale non-axisymmetric magnetic field of the Sun, and studying properties of the non-axisymmetric field can shed light on the origin of solar active regions. For instance, the magnitude and rotation rate of the large-scale non-axisymmetric magnetic field can bring the new information about the dynamo process inside the convection zone. The problem of non-axisymmetric perturbations has not been addressed in mean-field models of the large-scale solar dynamo. Theoretically it was argued that the solar dynamo is likely to operate in the so-called  $\alpha\Omega$  or  $\alpha^2\Omega$  regimes (Raedler 1986; Raedler et al. 1990). In these regimes the large-scale non-axisymmetric dynamo modes are linearly-stable because of a profound effect of the differential rotation on the large-scale magnetic field. Non-linear solar dynamo models show that a weak non-axisymmetric magnetic field can co-exists with the global axisymmetric field (Raedler et al. 1990; Moss 1999; Elstner & Korhonen 2005). The nonlinear models predict that the energy of the non-axisymmetric modes is only about  $10^{-4}$  of the energy of the axisymmetric component (Berdyugina et al. 2006). Observations on the Wilcox Solar Observatory (Duvall et al. 1979; Hoeksema 1995) find that the strength of the  $m=1$  non-axisymmetric mode can be about 1-2 G during epoch of solar maxims. The axisymmetric dipole has the same magnitude in the solar minims. It is likely that the origin of this non-axisymmetric field is related to decay of solar active regions. However it is unclear how the evolution

of such non-axisymmetric field may impact the solar dynamo process. The effect of the non-axisymmetric field on the large-scale dynamo has not been studied before.

In this paper we explore a response of a non-linear non-axisymmetric mean-field solar dynamo model to shallow non-axisymmetric perturbations with the magnetic field strength of 1G. We consider a fairly complete theoretical description of the mean electro-motive force taking into account the known properties of the solar convection zone and including the anisotropic turbulent effects due to the global rotation. The model includes the nonlinear magnetic buoyancy effect and two types of non-linearity of the  $\alpha$ -effect: due to the “algebraic” and “dynamical” quenching (Tworkowski et al. 1998). The algebraic quenching is due to the back-reaction of the dynamo-generated magnetic field on the helical turbulence. The dynamical quenching results from a magnetic helicity conservation condition (Kleeorin & Ruzmaikin 1982). We will show that given nonlinear non-axisymmetrical effects can reproduce the “flip-flop” phenomena and rotation rate of the active longitude on the Sun (Tuominen et al. 2002; Berdyugina et al. 2006; Gyenge et al. 2012).

## 2. Basic equations

Evolution of the large-scale magnetic field in perfectly conductive media is described by the mean-field induction equation (Krause & Rädler 1980; Moffatt 1978; Parker 1979):

$$\partial_t \langle \mathbf{B} \rangle = \nabla \times (\mathcal{E} + \langle \mathbf{U} \rangle \times \langle \mathbf{B} \rangle) \quad (1)$$

where  $\mathcal{E} = \langle \mathbf{u} \times \mathbf{b} \rangle$  is the mean electromotive force, with  $\mathbf{u}$  and  $\mathbf{b}$  are the turbulent fluctuating velocity and magnetic field respectively;  $\langle \mathbf{U} \rangle$  and  $\langle \mathbf{B} \rangle$  are the mean velocity and magnetic field. Our solution of the dynamo equation will follow the outline given earlier by Moss et al. (1991) and Moss (1999). For convenience we decompose the magnetic field into the axisymmetric, (hereafter  $\overline{\mathbf{B}}$ -field), and non-axisymmetric parts, (hereafter  $\tilde{\mathbf{B}}$ -field):

$\langle \mathbf{B} \rangle = \bar{\mathbf{B}} + \tilde{\mathbf{B}}$ . We assume that the mean flow is axisymmetric  $\langle \mathbf{U} \rangle \equiv \bar{\mathbf{U}}$ . Let  $\hat{\phi} = \mathbf{e}_\phi$  and  $\hat{\mathbf{r}} = r\mathbf{e}_r$  be vectors in the azimuthal and radial directions respectively, then we represent the mean magnetic field vectors as follows:

$$\langle \mathbf{B} \rangle = \bar{\mathbf{B}} + \tilde{\mathbf{B}} \quad (2)$$

$$\bar{\mathbf{B}} = \hat{\phi}B + \nabla \times (A\hat{\phi}) \quad (3)$$

$$\tilde{\mathbf{B}} = \nabla \times (\hat{\mathbf{r}}T) + \nabla \times \nabla \times (\hat{\mathbf{r}}S), \quad (4)$$

where  $A$ ,  $B$ ,  $T$  and  $S$  are scalar functions representing the axisymmetric and non-axisymmetric parts respectively. Assuming that  $A, B$  do not depend on longitude, Eqs(3, 4) ensure that the field  $\langle \mathbf{B} \rangle$  is divergence-free. Taking the scalar product of Eq(1) with vector  $\hat{\phi}$  we get the equations for the axisymmetric magnetic field components,

$$\partial_t B = \hat{\phi} \cdot \nabla \times (\boldsymbol{\varepsilon} + \bar{\mathbf{U}} \times \bar{\mathbf{B}}), \quad (5)$$

$$\partial_t A = \hat{\phi} \cdot (\boldsymbol{\varepsilon} + \bar{\mathbf{U}} \times \bar{\mathbf{B}}), \quad (6)$$

To get equation for  $T$  we take curl of the Eq(1) and then take scalar product with vector  $\hat{\mathbf{r}}$ . Similarly, equation for  $S$  is obtained by taking twice curl of Eq(1) and then the scalar product with vector  $\hat{\mathbf{r}}$ . The procedure is described in detail by Krause & Rädler (1980). Equations for the non-axisymmetric field are

$$\partial_t \Delta_\Omega T = \Delta_\Omega V^{(U)} + \Delta_\Omega V^{(\boldsymbol{\varepsilon})}, \quad (7)$$

$$\partial_t \Delta_\Omega S = \Delta_\Omega U^{(U)} + \Delta_\Omega U^{(\boldsymbol{\varepsilon})}, \quad (8)$$

where  $\Delta_\Omega = \frac{\partial}{\partial \mu} \sin^2 \theta \frac{\partial}{\partial \mu} + \frac{1}{\sin^2 \theta} \frac{\partial^2}{\partial \phi^2}$ ,  $\mu = \cos \theta$  and  $\theta$  is a polar angle, and

$$\Delta_\Omega V^{(U)} = -\hat{\mathbf{r}} \cdot \nabla \times \nabla \times (\bar{\mathbf{U}} \times \tilde{\mathbf{B}}), \quad (9)$$

$$\Delta_\Omega V^{(\mathcal{E})} = -\hat{\mathbf{r}} \cdot \nabla \times \nabla \times \mathcal{E}, \quad (10)$$

$$\Delta_\Omega U^{(U)} = -\hat{\mathbf{r}} \cdot \nabla \times (\bar{\mathbf{U}} \times \tilde{\mathbf{B}}), \quad (11)$$

$$\Delta_\Omega U^{(\mathcal{E})} = -\hat{\mathbf{r}} \cdot \nabla \times \mathcal{E}. \quad (12)$$

The scalar functions with superscript  $(U)$  contain contributions from the large-scale axisymmetric flows like differential rotation or meridional circulation. The integration domain include the solar convection zone from  $0.71$  to  $0.99R_\odot$ . The distribution of the mean flow is given by helioseismology (Howe et al. 2011 and Zhao et al. 2013). Profiles of the angular velocity and meridional circulation are illustrated in Figure 1.

Results of the global dynamo simulations (Schinnerer 2011; Brown et al. 2011; Brandenburg et al. 2012; Käpylä et al. 2012; Simard et al. 2013) show that agreement between the direct numerical simulation and mean-field models is good only if we have to take into account the full information about  $\mathcal{E}$ . We use the expressions for the mean electromotive force obtained by Pipin(2008). The calculations of the mean electromotive force are done using the mean-field magnetohydrodynamics framework and the so-called “minimal tau-approximation” (see, e.g., Blackman & Field 2002; Rädler et al. 2003; Brandenburg & Subramanian 2005). The tau-approximation suggests that the second-order correlations do not vary significantly on timescale  $\tau_c$  which corresponds to a typical turnover time of the convective flows. The theoretical calculations are performed for anelastic turbulent flows. They take into account the effects of density stratification, spatial inhomogeneity of the intensity of turbulent flows, and inhomogeneity of the large-scale magnetic fields. The effects of large-scale inhomogeneity of the turbulent flows and magnetic fields are computed to the first order of the Taylor expansion in terms of ratio  $\ell/L$ , where  $\ell$  is a typical spatial scale of the turbulence, and  $L$  is a spatial scale of the mean quantities.

The mean electromotive force,  $\mathcal{E}$ , is expressed as follows (Pipin, 2008):

$$\mathcal{E}_i = (\alpha_{ij} + \gamma_{ij}) \langle B \rangle_j - \eta_{ijk} \nabla_j \langle B \rangle_k. \quad (13)$$

where symmetric tensor  $\alpha_{ij}$  models the generation of the magnetic field by the  $\alpha$ - effect, antisymmetric tensor  $\gamma_{ij}$  controls the mean drift of the large-scale magnetic fields in turbulent medium, tensor  $\eta_{ijk}$  governs the turbulent diffusion. We take into account the effect of rotation and magnetic field on the mean-electromotive force (see Appendix for details). To determine a unique solution of Eqs.(5-8) we apply the following gauge (see, e.g., Krause & Rädler 1980; Bigazzi & Ruzmaikin 2004a):

$$\int_0^{2\pi} \int_{-1}^1 S d\mu d\phi = 0, \quad \int_0^{2\pi} \int_{-1}^1 T d\mu d\phi = 0. \quad (14)$$

The same gauge is used in Eqs(9-12).

## 2.1. Nonlinear interaction of the axisymmetric and non-axisymmetric modes

Interaction between the axisymmetric and non-axisymmetric modes in the mean-field dynamo models can be due to nonlinear dynamo effects, for example  $\alpha$ -effect, (Krause & Rädler 1980; Moss 1999). In model t  $\alpha$  effect takes into account the kinetic and magnetic helicities in the following form:

$$\alpha_{ij} = C_\alpha \sin^2 \theta \psi_\alpha(\beta) \alpha_{ij}^{(H)} \eta_T + \alpha_{ij}^{(M)} \frac{\langle \chi \rangle \tau_c}{4\pi \bar{\rho} \ell^2} \quad (15)$$

where  $C_\alpha$  is a free parameter which controls the strength of the  $\alpha$ - effect due to turbulent kinetic helicity;  $\alpha_{ij}^{(H)}$  and  $\alpha_{ij}^{(M)}$  express the kinetic and magnetic helicity parts of the  $\alpha$ -effect, respectively;  $\eta_T$  is the magnetic diffusion coefficient, and  $\langle \chi \rangle = \langle \mathbf{a} \cdot \mathbf{b} \rangle$  ( $\mathbf{a}$  and  $\mathbf{b}$  are the fluctuating parts of magnetic field vector-potential and magnetic field vector). Both the  $\alpha_{ij}^{(H)}$  and  $\alpha_{ij}^{(M)}$  depend on the Coriolis number  $\Omega^* = 4\pi \frac{\tau_c}{P_{rot}}$ , where  $P_{rot}$  is the rotational period,  $\tau_c$  is the convective turnover time, and  $\ell$  is a typical length of the convective flows

(the mixing length). A theoretical justification for the latitudinal factor,  $\sin^2 \theta$ , in Eq(15) was given by Kleeorin & Rogachevskii (2003). Function  $\psi_\alpha(\beta)$ , controls the so-called “algebraic” quenching of the  $\alpha$ - effect where  $\beta = |\langle \mathbf{B} \rangle| / \sqrt{4\pi\bar{\rho}u'^2}$ ,  $u'$  is the RMS of the convective velocity. For the case of the strong magnetic field,  $\beta \gg 1$ ,  $\psi_\alpha \sim \beta^{-2}$ . The interaction between the axisymmetric and non-axisymmetric dynamo modes via  $\psi_\alpha(\beta)$  is because both modes contribute to parameter  $\beta$ . Also for the case  $\beta > 1$ , the latitudinal profile of the  $\alpha$  effect changes. This can affect the dynamo conditions for excitation of the non-axisymmetric modes. Raedler et al. (1990) and Moss (1999) discussed the evolution of non-axisymmetric magnetic field in a simple dynamo model with such “algebraic” quenching.

The dynamical quenching is caused by the magnetic helicity conservation (see, Kleeorin & Ruzmaikin 1982). This effect was discovered by Frisch et al. (1975) and Pouquet et al. (1975). Contribution of the magnetic helicity to the  $\alpha$ -effect is expressed by the second term in Eq.(15). The magnetic helicity density of turbulent field,  $\langle \chi \rangle = \langle \mathbf{a} \cdot \mathbf{b} \rangle$ , is governed by the conservation law (Hubbard & Brandenburg 2012; Pipin et al. 2013):

$$\frac{\partial \langle \chi \rangle^{(tot)}}{\partial t} = -\frac{\langle \chi \rangle}{R_m \tau_c} - 2\eta \langle \mathbf{B} \rangle \cdot \langle \mathbf{J} \rangle - \nabla \cdot \mathcal{F}^\chi, \quad (16)$$

where  $\langle \chi \rangle^{(tot)} = \langle \chi \rangle + \langle \mathbf{A} \rangle \cdot \langle \mathbf{B} \rangle$  is the total magnetic helicity density of the mean and turbulent fields,  $\mathcal{F}^\chi = -\eta_\chi \nabla \langle \chi \rangle$  is the diffusive flux of the turbulent magnetic helicity, and  $R_m$  is the magnetic Reynolds number. The coefficient of the turbulent helicity diffusivity,  $\eta_\chi$ , is chosen ten times smaller than the isotropic part of the magnetic diffusivity (Mitra et al. 2010):  $\eta_\chi = \frac{1}{10}\eta_T$ . Similarly to the magnetic field, the mean magnetic helicity density can be formally decomposed into the axisymmetric and non-axisymmetric parts:  $\langle \chi \rangle^{(tot)} = \bar{\chi}^{(tot)} + \tilde{\chi}^{(tot)}$ . The same can be done for the magnetic helicity density of the turbulent field:  $\langle \chi \rangle = \bar{\chi} + \tilde{\chi}$ , where  $\bar{\chi} = \overline{\mathbf{a} \cdot \mathbf{b}}$  and  $\tilde{\chi} = \langle \mathbf{a} \cdot \tilde{\mathbf{b}} \rangle$ . Then we have,

$$\bar{\chi}^{(tot)} = \bar{\chi} + \overline{\mathbf{A} \cdot \mathbf{B}} + \overline{\tilde{\mathbf{A}} \cdot \tilde{\mathbf{B}}}, \quad (17)$$

$$\tilde{\chi}^{(tot)} = \tilde{\chi} + \overline{\mathbf{A} \cdot \tilde{\mathbf{B}}} + \overline{\tilde{\mathbf{A}} \cdot \mathbf{B}} + \overline{\tilde{\mathbf{A}} \cdot \tilde{\mathbf{B}}}, \quad (18)$$

Evolution of the  $\bar{\chi}$  and  $\tilde{\chi}$  is governed by the corresponding parts of Eq(16). Thus, the model takes into account contributions of the axisymmetric and non-axisymmetric fields in the whole magnetic helicity density balance, providing a non-linear coupling. We see that the  $\alpha$ -effect is dynamically linked to the longitudinally averaged magnetic helicity of the non-axisymmetric  $\tilde{\mathbf{B}}$ -field, which is the last term in Eq(17). Thus, the nonlinear  $\alpha$ -effect is non-axisymmetric and it results to coupling between evolution of axisymmetric and non-axisymmetric modes. The coupling works in both directions. For instance, the azimuthal  $\alpha$ -effect results to  $\mathcal{E}_\phi = \alpha_{\phi\phi} \langle B_\phi \rangle$ . If we denote the non-axisymmetric part of the  $\alpha_{\phi\phi}$  by  $\tilde{\alpha}_{\phi\phi}$  then the mean electromotive force is  $\bar{\mathcal{E}}_\phi = \bar{\alpha}_{\phi\phi} \bar{B}_\phi + \overline{\tilde{\alpha}_{\phi\phi} \tilde{B}_\phi}$ . This introduces a new source in Eq(6) which is usually ignored in the axisymmetric dynamo models.

The magnetic buoyancy is another nonlinear effect which is believed to be important in the large-scale dynamo. The part of the mean electro-motive force which is responsible for the magnetic buoyancy reads (Kichatinov & Pipin 1993):

$$\boldsymbol{\mathcal{E}}^{(\beta)} = V_\beta \hat{\mathbf{r}} \times \mathbf{B}, \quad (19)$$

where  $V_\beta = C_\beta \frac{\alpha_{MLT} u'}{\gamma} \beta^2 K(\beta)$ ,  $u'$  is the RMS convection velocity,  $K(\beta)$  is given in Appendix,  $\gamma$  is the adiabatic exponent,  $\alpha_{MLT}$  is the mixing-length theory parameter,  $C_\beta$  is a free parameter to switch on/off the effect in the model. For the case  $\beta \ll 1$ ,  $K \sim 1$  and the upflow velocity,  $V_\beta$ , is proportional to the pressure of large-scale magnetic field. Similarly to the  $\alpha$  effect, the  $V_\beta$  is non-axisymmetric and it results to source terms in Eqs(5,6). Note that the advection of the large-scale magnetic field by the magnetic buoyancy reduces concentration of the magnetic field near the bottom of the convection zone and increases the field strength near the top.

## 2.2. Parameters of the convection zone and numerical procedure

The distribution of the turbulent parameters, such as the typical convective turn-over time,  $\tau_c$ , the mixing length,  $\ell$ , the RMS convection velocity,  $u'$ , are taken from the solar interior model of Stix (2002). We define the mixing-length  $\ell = \alpha_{\text{MLT}} |\Lambda^{(p)}|^{-1}$ , where  $\Lambda^{(p)} = \nabla \log \bar{p}$  is the inverse pressure scale, and the mixing-length parameter  $\alpha_{\text{MLT}} = 2$ . The profile of the turbulent diffusivity is given in form  $\eta_T = C_\eta \frac{u'^2 \tau_c}{3 f_{ov}(r)}$ , where  $f_{ov}(r) = 1 + \exp[50(r_{ov} - r)]$ ,  $r_{ov} = 0.725R_\odot$  controls quenching of the turbulent effects near the bottom of the convection zone, which is  $r_b = 0.715R_\odot$ . Coefficient  $C_\eta$ , ( $0 < C_\eta < 1$ ) is a free parameter which controls the efficiency of mixing of the large-scale magnetic field by the turbulence. It is usually employed to tune the period of the dynamo cycle.

The numerical scheme employs the spherical harmonics decomposition for the non-axisymmetric part of the problem, i.e., the scalar functions T and S in Eqs(7,8) are represented in the form:

$$T(r, \mu, \phi, t) = \sum \hat{T}_{l,m}(r, t) P_l^{|m|} \exp(im\phi), \quad (20)$$

$$S(r, \mu, \phi, t) = \sum \hat{S}_{l,m}(r, t) P_l^{|m|} \exp(im\phi), \quad (21)$$

where  $P_l^m$  is the associated Legendre function of degree  $l \geq 1$  and order  $m \geq 1$ . The simulations which we will discuss include 600 spherical harmonics ( $l_{max} = 28$ ). Note that  $\hat{S}_{l,-m} = \hat{S}_{l,m}^*$  and the same for  $\hat{T}$ . We employ the pseudo-spectral approach for integration along latitude. The second-order finite differences are used for discretization the radial direction. The numerical integration is carried out in latitude from the pole to pole and in radius from  $r_b = 0.715R_\odot$  to  $r_e = 0.99R_\odot$ . All the nonlinear terms are calculated in the real space. The transformation between the spectral spherical harmonic and the real 3D space was done using the Intel Fortran FFT library. We implemente the ideas of Muciaccia et al. (1997) to speed-up the transform calculations. At the bottom of the convection zone weset up a perfectly conducting boundary condition for the axisymmetric magnetic field,

and for the non-axisymmetric field we set the functions  $S$  and  $T$  to zero. At the top of the convection zone the poloidal field is smoothly matched to the external potential field, and the boundary conditions for toroidal field allow its penetration to the surface as discussed by Moss et al. (1991) and Pipin & Kosovichev (2011):

$$\delta \frac{\eta_I}{r_e} B + (1 - \delta) \mathcal{E}_\theta = 0, \quad (22)$$

$$\frac{\delta}{R} T - (1 - \delta) \frac{\partial T}{\partial r} = 0 \quad (23)$$

where parameter  $\delta = 0.99$ .

The particular choice of the parameters which we employ in the model is based on the case of the solar dynamo model discussed in our previous papers (see, e.g, Pipin & Kosovichev 2014). The free parameters are  $C_\alpha = 0.04$ , (see Eq(A5)),  $C_\delta = \frac{1}{3} C_\alpha$ , (see Eq(A1)),  $C_\eta = \frac{1}{15}$  and the anisotropy parameter  $a = 3$  (see Eq(A1)). The given  $C_\alpha$  is about 30% above the dynamo generation threshold. For the chosen values of  $C_\eta$  and  $a$  the magnitude of the turbulent diffusion in the solar sub-surface shear level at  $r = 0.9R_\odot$  is about  $10^9 \text{m}^2 \text{s}^{-1}$  which is in agreement with observations (see, Abramenko et al. 2011). The magnetic helicity conservation is determined by the magnetic Reynolds number  $R_m$ , for which we considered values:  $10^4$ -  $10^6$ .

### 2.3. Initial conditions

In our first runs the weak initial field, which consisted of a superposition sum of polar and equatorial dipoles with strength of 0.01G, evolved to a state in which the axisymmetric dynamo regime dominates. In this regime, the typical strength of the axisymmetric toroidal field in the convection zone is about 1kG. The non-axisymmetric field is rather weak with the strength about  $10^{-6}$ G. This means that in our model the non-axisymmetric

magnetic field is linearly stable, unless we force the dynamo governing parameters to be non-axisymmetric, e.g., like in the paper by Bigazzi & Ruzmaikin (2004a).

Exploring the nonlinear solutions we found that the evolution of the non-axisymmetric field depends on the initial conditions which includes the strength and geometry of both the axisymmetric  $\bar{\mathbf{B}}$ -field and the non-axisymmetric  $\tilde{\mathbf{B}}$ -field. The evolution of the large-scale magnetic field depends on the presence of the meridional circulation, too.

In the following section we present results for the non-axisymmetric dynamo which was excited by seeding a finite-amplitude non-axisymmetric  $\tilde{\mathbf{B}}$ -field in the developed axisymmetric dynamo regime. Such non-axisymmetric perturbations can be developed either due to evolution of active regions or due to instabilities not described by the mean-field theory (e.g., Dikpati & Gilman 2001). For the seed field we consider a non-symmetric relative to the equator perturbation represented by the sum of the equatorial dipole ( $l=1$ ,  $m=1$ ) and quadrupole ( $l=2$ ,  $m=1$ ) components. In Eq(21) we define

$$S_{1,1} = \left(1 - \operatorname{erf}\left(\frac{(r_s - r_e)}{d}\right)\right) \frac{r_e}{r}, \quad (24)$$

$$S_{1,2} = \left(1 - \operatorname{erf}\left(\frac{(r_s - r_e)}{d}\right)\right) \left(\frac{r_e}{r}\right)^2, \quad (25)$$

where,  $r_e = 0.99R$ ,  $r_s = 0.9R$  is the bottom of the subsurface shear layer,  $d = 0.02R$ .

The other  $S_{l,m}$  and  $T_{l,m}$  are zero at the moment of seed. In these simulations the initial non-axisymmetric field is forced to be shallow. The depth of the non-axisymmetric perturbation influences evolution of the axisymmetric dynamo.

### 3. Results

Figure 2 illustrates the geometry of the axisymmetric and non-axisymmetric field just before initialization of the non-axisymmetric perturbation. Figure 3 illustrates the evolution of the axisymmetric magnetic field before and after the seed of the non-axisymmetric

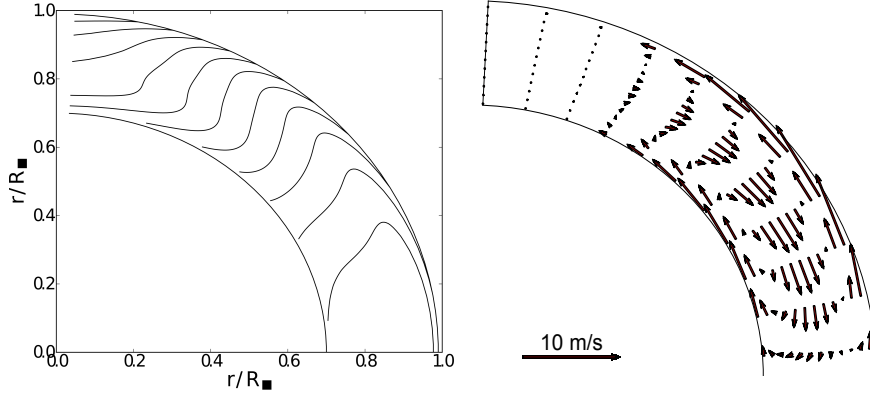


Fig. 1.— Distribution of the angular velocity (left) and the meridional circulation in the convection zone (right).

Table 1: Summary of the dynamo models and their parameters.

Components	M1	M2
$\alpha_{ij}$ -effect	Eqs.(15,16,A6,A7)	same
$\eta_{ijk}$ -diffusivity	Eqs.(A1)	same
$\gamma_{ij}$ -pumping	Eqs.(A17)	same
circulation	no	$\bar{U} = 10\text{m/s}$
free parameters	$C_\alpha = 0.04, C_\delta = C_\alpha/3,$ $C_\eta = 0.06, C_v = 1, a=3,$ $C_\beta = 1$ and $C_\beta = C_\eta,$ $R_m = 10^{4-6}, \alpha_{MLT} = 2$	$C_\alpha = 0.05, C_\beta = 1$ , others are same as in M1

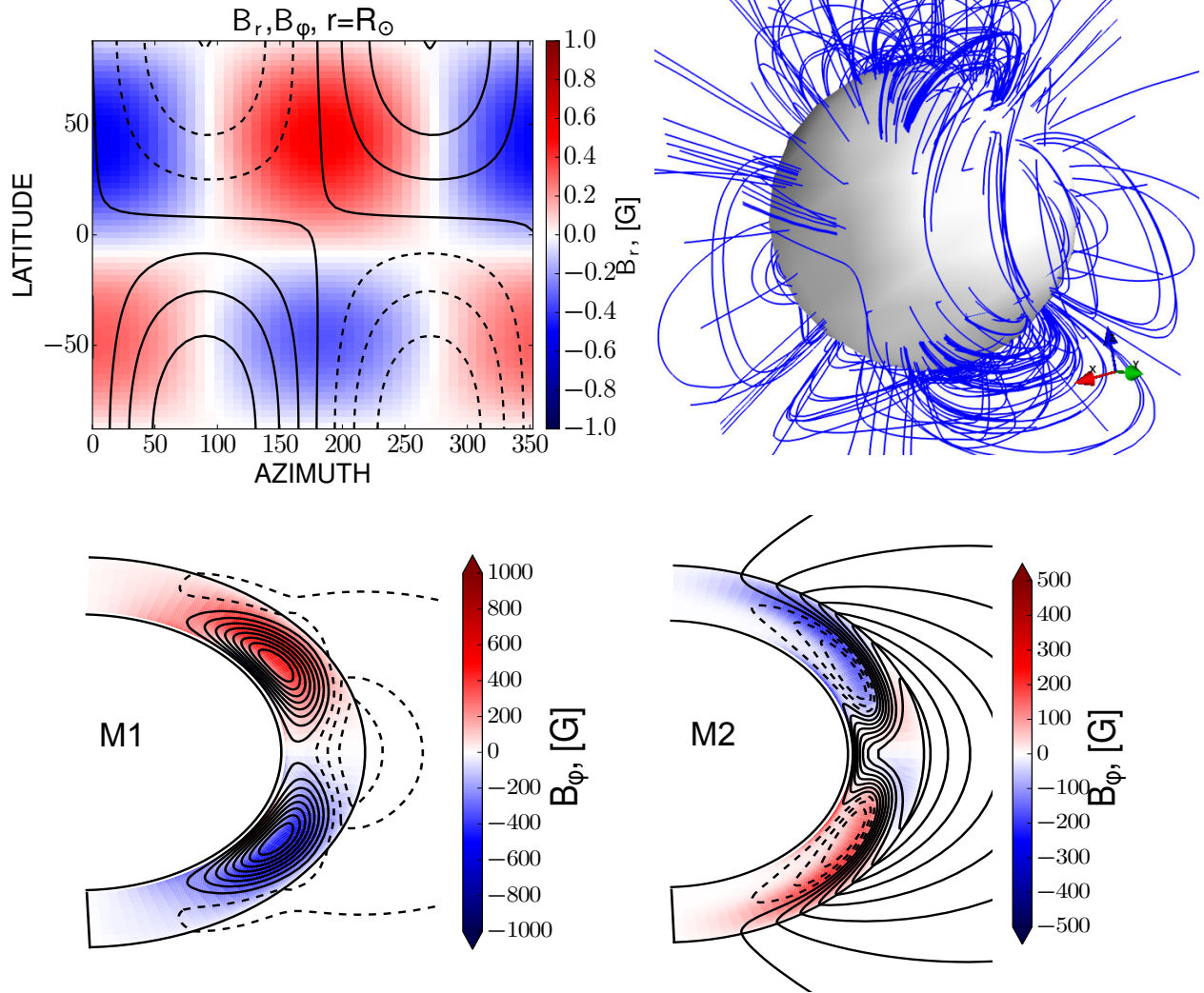


Fig. 2.— Initial non-axisymmetric field and the large-scale magnetic fields in the model M1, M2 at the moment of seed the non-axisymmetric perturbation

perturbation for two models with and without the meridional circulation. We show the time-latitude diagrams for the toroidal magnetic field in the subsurface shear layer and the radial magnetic field at the surface. In the model with the meridional circulation the toroidal magnetic field is shown for the middle of the convection zone (see Pipin & Kosovichev 2013). The evolution in the radial direction is shown for  $30^\circ$  latitude in the Northern hemisphere. We simulate the sunspot number  $W$  using the ansatz (Pipin et al. 2012):

$$W(t) = \langle B_{\max} \rangle_{SL} \exp\left(-\frac{B_0}{\langle B_{\max} \rangle_{SL}}\right), \quad (26)$$

where in the model M1  $\langle B_{\max} \rangle_{SL}$  is the maximum strength of the toroidal magnetic field averaged over radius in the subsurface layers in the range of  $0.9 - 0.99R_\odot$ , and in the model M2 it is the same for the middle of the convection zone;  $B_0$  a characteristic strength of the toroidal magnetic field,  $B_0 = 800\text{G}$ .

The models show that the given non-axisymmetric perturbation produces a transient cycle both in the model M1 and in the M2. In the Northern hemisphere, where the perturbation is stronger the simulated sunspot number cycle is higher than in the Southern hemisphere. The perturbation affects the reversal of the polar magnetic fields. In the Northern hemisphere the polar reversal goes earlier than in the Southern hemisphere where we see multiple reversals. The models show a time shift about 2 years for the polar reversals in the Northern and Southern hemispheres. We find that these phenomena depends on the depth of perturbation (parameters,  $r_s$  and  $d$  in Eq(24)). For instance, polar reversal happens earlier in the Southern hemisphere than in the Northern one for  $r_s = 0.95$ . We also see that in model M1 the cycle return quickly to the previously established axisymmetric state. In model M2 with the meridional circulation the restoration process takes longer than in model M1. In that model the normal cycles are restored about 40 year after perturbation. This is for  $R_m = 10^4$ . For the higher  $R_m$  the relaxation in both models goes in the same time-scales. Figure 4 illustrates results in model M1 for  $R_m = 10^{4,6}$  and for model M1

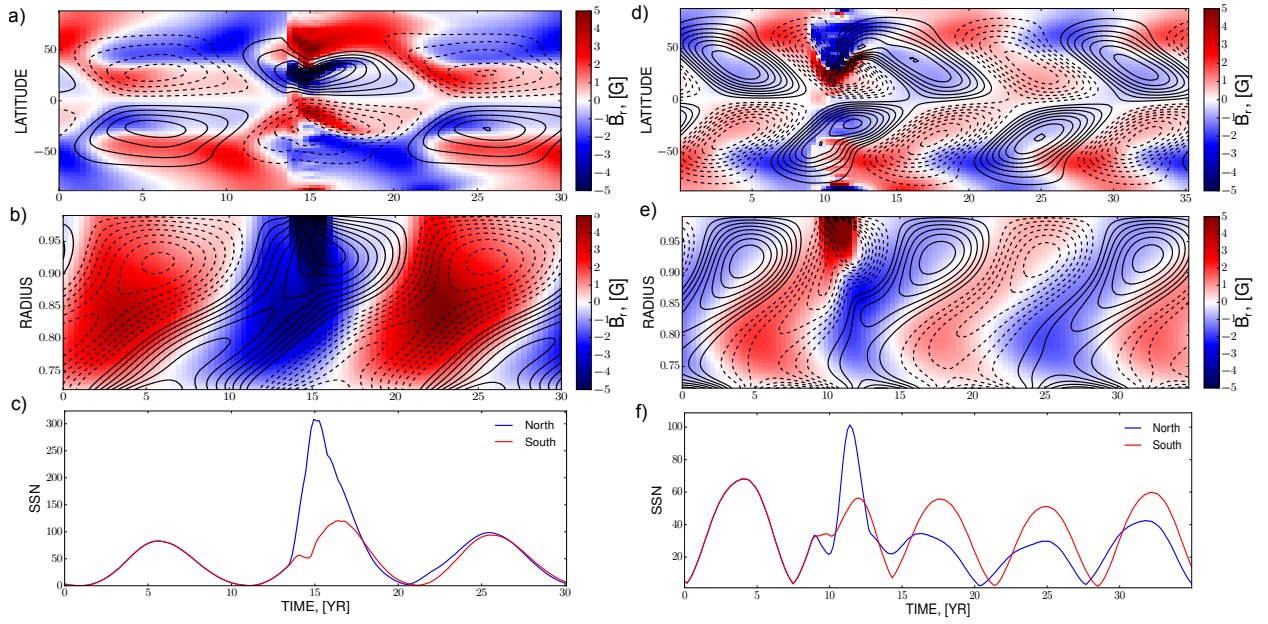


Fig. 3.— Time-latitude diagram (a), the simulated sunspot number (b), the evolution of the azimuth of the  $T_1$  antisymmetric mode (c) and evolution of the absolute strength of the axisymmetric and the non-axisymmetric parts of the large-scale toroidal magnetic field.

with a reduced magnetic buoyancy effect ( $C_\beta = C_\eta$ ). The developed axisymmetric dynamo regime which is employed at the beginning of evolution series shown in Figure e 4 is related to the the case  $R_m = 10^4$  and  $C_\beta = 1$ . This explains why magnetic cycles in model M1 with  $C_\beta = C_\eta$  and  $R_m = 10^6$  do not relax to original cycle amplitude. The model with a reduced magnetic buoyancy shows the factor 2 smaller magnitude of  $T_{1,1}$  mode after relaxation. The mode  $T_{1,1}$  shows larger variations in case of  $R_m = 10^6$  than in case of  $R_m = 10^4$  after relaxation.

The restoration of the initial of the axisymmetric magnetic field evolution does not mean that the non-axisymmetric field completely dissipates. Figures 5(a,c) and 6(a,c) show that a low strength non-axisymmetric field is maintained in the model. We find that the strength of the toroidal field T-potentials is reduced from about 10G at the maximum to 0.01G after the relaxation. Even such a low strength non-axisymmetric magnetic field can produce some interesting phenomena which may be related to solar observations.

Figures 5(b,d) and 6(b,d) shows the evolution of longitude of maximum of the large-scale toroidal field and the latitude-longitude position of maxims of the large-scale toroidal magnetic field strength at the subsurface shear layer. The model M1 (without circulation) show the periodic changes of the longitudes to  $180^\circ$  degrees during the magnetic cycle decay. The change of the longitude is accompanied by the change of the hemispheric position of maximum. Thus, the orientation of the global non-axisymmetric field is reversed every cycle during the minims of the toroidal magnetic field . This behavior may correspond to the flip-flop phenomenon of the active longitudes observed in stellar magnetic cycles (Berdyugina 2004).

Model M2 which includes the effect of meridional circulation has no the stable positions of the azimuth of the non-axisymmetric magnetic field. Figures 5(a) and 6(a) clarify the reason for this. The effect disappears because the circulation mixes the magnetic field in

from the subsurface shear layer with the magnetic field of the deep interior with period that approximately corresponds to the period of the magnetic cycle. We see that oscillations of the  $S_1$  and  $T_1$  harmonics have a  $\pi/2$  phase shift. Thus for a persistent appearance of the active longitude the phases of the  $S_1$  and  $T_1$  harmonics should be consistent. The model M2 shows the continues drift of the longitude of the large-scale toroidal magnetic field strength in the course of the magnetic activity evolution.

Figure 7 shows snapshots of the axisymmetric and non-axisymmetric fields after a half-year evolution of the initial perturbation. We also show configuration of the external potential field. This period of time corresponds a maximum of the toroidal magnetic field in the upper part of the convection zone, and the epoch of the polar field reversal. The non-axisymmetric part of the field is concentrated to the surface (as the initial field). The longitude -latitude diagram shows distributions of the large-scale magnetic field (including the axisymmetric and non-axisymmetric parts). It illustrates how the differential rotation stretches the initial magnetic field configuration (cf., Fig2a). Snapshots show the large-scale unipolar regions which extend from equator to poles. The increasing the of the non-axisymmetric magnetic field in the polar regions results in the twisted field lines going from the polar caps.

However, the magnetic field configuration returns to almost axisymmetric state after 5 years from initialization of the non-axisymmetric perturbation. Figure 9 illustrates the snapshots of the magnetic field configuration during the decaying phase of the magnetic cycle in model M1. We see that the non-axisymmetric toroidal field is distributed over the convection zone having maxims at the bottom of the convection zones and in the near equatorial region. The strength of the non-axisymmetric field is much smaller than the axisymmetric one. Model M2 has long overlaps between the subsequent cycles. Snapshots for this model are shown in Fig.9(bottom) for the growing phase of the cycle. The snapshots

show the situation when the symmetric about the equator  $m=1$  mode dominates at the surface. In the deep layers the general distribution of the non-axisymmetric magnetic field is close to model M1.

The relaxed stage of the evolution begins about 15 years after the initialization of the non-axisymmetric magnetic field in the model M1 (see Fig.5). The relaxation time of model M2 is about 20 years. In the relaxed stage of evolution the non-axisymmetric field is concentrated at the top of the convection zone like on the snapshots shown by Figures 7 and 8 (also see the Figures 5(a) and 6(a)). The antisymmetric modes  $m=1$  dominates in the both models. Thus

Figure 10 shows the power spectra of FFT transform for time series of the equatorial dipole in the inertial rotating frame for the three levels of the solar convection zone. The time series cover the period about 5 year after the initialization of the non-axisymmetric field in the models. At the initialization time the equatorial dipole was rotating with a period of 27.26 days, which corresponds to the latitude of maximum of the initial perturbation. For model M1 it is found that in the subsurface shear layer the equatorial dipole rotates with periods of 25.1-25.5 days. This corresponds to rotation rate of the subsurface shear layer at the  $30^\circ$  latitude. At the surface it rotates with the period about 25.7 days and at the bottom of the convection zone it rotates with the period of 25.1 days. The origin of these rotational periods has to be studied further. It seems that periods of rotation follows the rotation profile in the solar convection zone. In model M2 the meridional circulation mix all the layers of the convection zone producing the unique maximum equal to period of 25.4 days, which correspond to latitude about  $30^\circ$  at the  $r = 0.9R$ . Comparison snapshots of the non-axisymmetric field in Fig.8(c) and Fig9(f) confirms this idea. In model M1 distribution of the toroidal magnetic field in equatorial regions follows the rotational profile shown in Fig.1. Model M2 loses this effects because of the meridional circulation.

#### 4. Discussion and Summary

In the paper we explored the evolution of a non-axisymmetric perturbation in the mean-field solar-type dynamo models. The models are kinematic with respect to the mean flow. The distribution of the mean flow is taken from the recent results of helioseismology. The rotational profile inferred by helioseismology includes the part of tachocline and the subsurface shear layer. We use the double-cell meridional circulation pattern which was suggested by the helioseismology results of Zhao et al. (2013). To abetter understand the effect of meridional circulation we studied models with and without meridional circulation. The non-axisymmetric dynamo model takes into account the mean turbulent electromotive force in a fairly complete form. We take into account the tensor form of the  $\alpha$ -effect, the turbulent diffusivity and the turbulent pumping effects which are anisotropic because of the effects of the global rotation. The mean electromotive force which is employed in the non-axisymmetric part of the model is the same as for the axisymmetric part except the  $\delta$ -effect (Rädler 1969). This effect has not been included in our non-axisymmetric dynamo model and will be investigated separately.

Earlier it was found that excitation of the large-scale non-axisymmetric field on the Sun and solar-type stars is possible due to the non-linear  $\alpha$ -effect (Raedler et al. 1990; Moss et al. 1991; Moss 1999). Those models predicted a rather weak non-axisymmetric field for the solar case. The main reason for this is that the differential rotation on the Sun is rather strong. It efficiently cascades the non-axisymmetric field to the small-scales at which it dissipated by the turbulent diffusion dissipate it before the dynamo instability start (Raedler et al. 1990). The non-linear  $\alpha$ -effect couples the evolution of the axisymmetric and the non-axisymmetric parts of the field. Thus the non-axisymmetric dynamo can be maintained in expense of the energy of the axisymmetric magnetic field.

In the paper we considered the models with the magnetic helicity and magnetic

buoyancy effects, which were not studied before in non-axisymmetric dynamo models. The study confirms the previous findings of Moss (1999) that the regular part of the non-axisymmetric dynamo is rather weak if we start from a weak initial non-axisymmetric seed field. We have to notice that our models can be characterized as weakly non-linear because the parameter of the  $\alpha$ -effect in the model is only 30% above the dynamo instability threshold. Also the magnetic helicity conservation efficiently prevents the generation of the magnetic field of the super-equipartition strength (Brandenburg & Käpylä 2007; Hubbard & Brandenburg 2012). Thus the low-strength non-axisymmetric magnetic field can be explained by the linear stability of the non-axisymmetric field and the weak non-linearity of the dynamo system.

The paper concentrates on illustrating the effect of the non-axisymmetric perturbation on the axisymmetric dynamo and the subsequent evolution of the non-axisymmetric magnetic field. In addition to the models M1 and M2 presented in the paper, we run the models for the different case of the initial conditions including the change of the spatial distribution of non-axisymmetric perturbation and the change of the initialization time to the different epoch of the magnetic cycle. In model M1 the effect of perturbation is greatest when it is initiated at the growing phase of the cycle. Also, the impact of perturbation and the amplitude of the non-axisymmetric after relaxation increase with increase of the perturbation depth. On the other hand if the perturbation in form the Eq(24) is localized near the bottom of the convection zone, it produces only a little effect on the large-scale dynamo. This conclusion can be changed if we would consider the non-local  $\alpha$ -effect which related the generation of the poloidal field on the surface with toroidal magnetic field at the bottom of the convection zone. This question is out of the scope of the paper.

The model M2 has a long overlap between the subsequent cycle (see Fig.3). Therefore we did not investigate in details the question about impact of initiation phase of perturbation

on the dynamo. The other conclusions which we mentioned discussing the effects of initial conditions for the model M1 are valid for the model M2 as well.

It seems that effect of the magnetic helicity conservation is the most important to preserve the non-axisymmetric field from decay to zero. Our model relies on the simplified approach to the problem. The evolution of the magnetic helicity density in the model depends on the effective magnetic Reynolds number  $R_m$  and the turbulent diffusivity  $\eta_\chi$ . For the latter value we use results of the numerical simulation of Mitra et al. (2010), who found that  $\eta_\chi \approx \frac{1}{10}\eta_T$ . We made additional runs varying  $R_m$  in the range  $10^4$  to  $10^6$ . It is found that the magnitude of transient cycle is about fifty percent larger in case of  $R_m = 10^4$  than in the case of  $R_m = 10^6$ . The relaxation goes in the same way as in case of  $R_m = 10^4$ . However in the case of  $R_m = 10^6$  the magnetic cycles which are follows the transient cycle have about 20% smaller amplitude than the original cycle. This happens because the magnetic helicity conservation, which is better in case  $R_m = 10^6$  than in case of  $R_m = 10^4$ , quenches of the generation magnetic field by the  $\alpha$ -effect.

Also, our models includes the nonlinear effect of magnetic buoyancy. It was never discussed in the mean-field non-axisymmetric dynamo. It is found that the strength of the non-axisymmetric field after relaxation is factor of two magnitude smaller if the magnetic buoyancy is switched off. Meanwhile decreasing the magnetic buoyancy increase the amplitude of the axisymmetric field.

The models without meridional circulation show the persistent “active longitudes” when the relaxation phase of evolution is passed. The models show that the non-axisymmetric field undergoes flip-flops around these longitudes during the decaying phase of the magnetic cycle. The origin of these longitudes and flip-flop phenomena in nonlinear non-axisymmetric dynamo where discussed in details by Moss (2004) (see, also, discussion in Berdyugina et al. 2006). In our calculations the active longitude is fixed when the phases of evolution of  $T_1$

and  $S_1$  modes are consistent (goes in phase or in anti-phase). The flip-flop occurs when the orientation of the equatorial dipole change the sign. If this effect is accompanied by the equatorial symmetry variations of the axisymmetric magnetic field then the orientation of the large-scale magnetic field changes to  $180^\circ$ .

Rotation of the non-axisymmetric magnetic field harmonics is rather important for the purpose of diagnostic. Bigazzi & Ruzmaikin (2004b) found the periods of 26.18 days in their linear non-axisymmetric model with the  $\alpha$ -effect distributed in the convection zone. They found a period of 26.7 days for the model with the  $\alpha$ -effect concentrated to the top of the convection zone. Our model without meridional circulation shows the different periods for the  $T_1$  (and same for the  $S_1$ ) for the different levels of the solar convection zone. The  $T_1$  at the  $r = 0.9R$  has periods from 25.1 to 25.5 days. At the bottom of the convection zone it rotates with period about 25.1 days. This is due to generation of the mode in the subsurface shear layer and its subsequent redistribution to equatorial regions by differential rotation. At the surface the given mode rotates slower with period 25.7 days. Circulation mixes the modes from all the layers of the convection zone producing the unique maximum equal to period of 25.4 days, which correspond to latitude about  $30^\circ$  at the  $r = 0.9R$ . The give periods are related to period of relaxation of the non-axisymmetric perturbation. After relaxation is passed the active longitude is rotating with the sidereal period 27.2 days.

The paper illustrates the first results of the nonlinear non-axisymmetric mean-field dynamo model. The axisymmetric part of the model is based on our previous results. For the first time we demonstrate that nonlinear coupling between the asymmetric and the non-axisymmetric field can impact the generation of the axisymmetric field. The effect depends strongly on the dynamo mechanisms involved in the problem, the spatial distribution of perturbation, conditions of the dynamo processes at the time and how well the magnetic helicity is conserved in the system. Those factors determine the subsequent

evolution of the dynamo system including the cycle of the axisymmetric dynamo, evolution and rotation of the non-axisymmetric modes of the large-scale magnetic fields.

We conclude as follows:

- In the solar dynamo models non-axisymmetrical perturbations decay and can be maintained only at low amplitude because of nonlinear turbulent effects
- Relaxation of perturbation depends on the dissipation of magnetic helicity.
- Without meridional circulation non-axisymmetric models can show the flip-flop phenomenon. The solar-type meridional circulation destroys this effect.

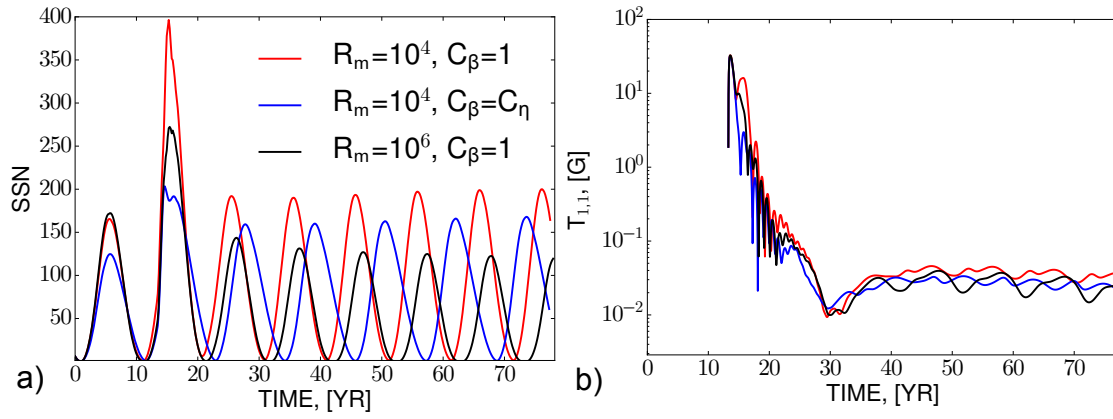


Fig. 4.— Evolution of the simulated sunspot number (a) and  $T_{1,1}$  harmonic (b) in the model M1 for the different values of the parameter  $R_m$  and  $C_\beta$ .

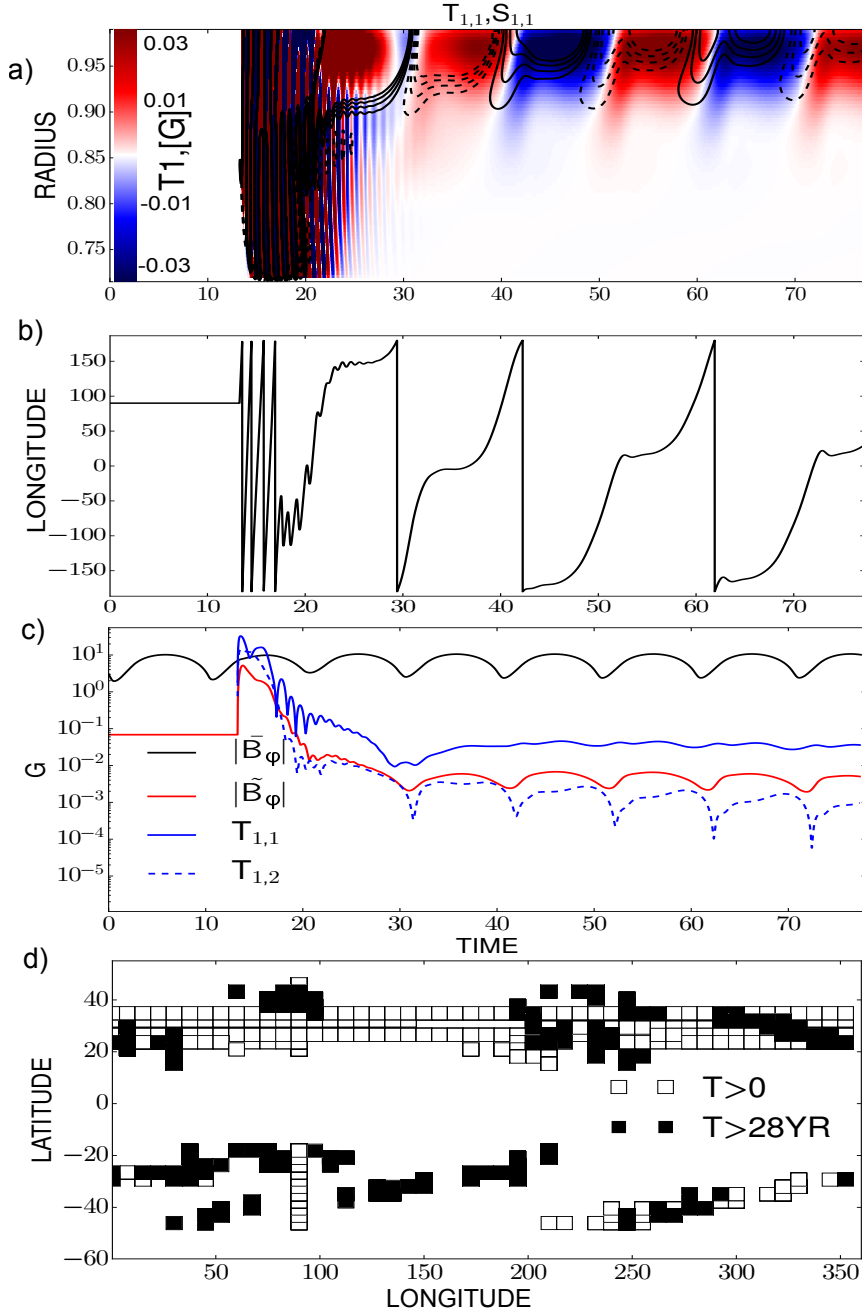


Fig. 5.— The model M1: a) the time-radius evolution of the modes  $T_{1,1}$ (background image) and  $S_{1,1}$ (contours in the same range of values as for  $T_{1,1}$ ) modes; b) evolution of longitude of maximum of the large-scale toroidal field, c) the mean strength of the near-surface axisymmetric and non-axisymmetric toroidal magnetic field and the strength of the  $m=1$  T-potentials, d) position of maxims of the total toroidal magnetic field strength at the sub-surface shear layer ( $r=0.92R$ ). There the filled squares are related to period of time after 28 year

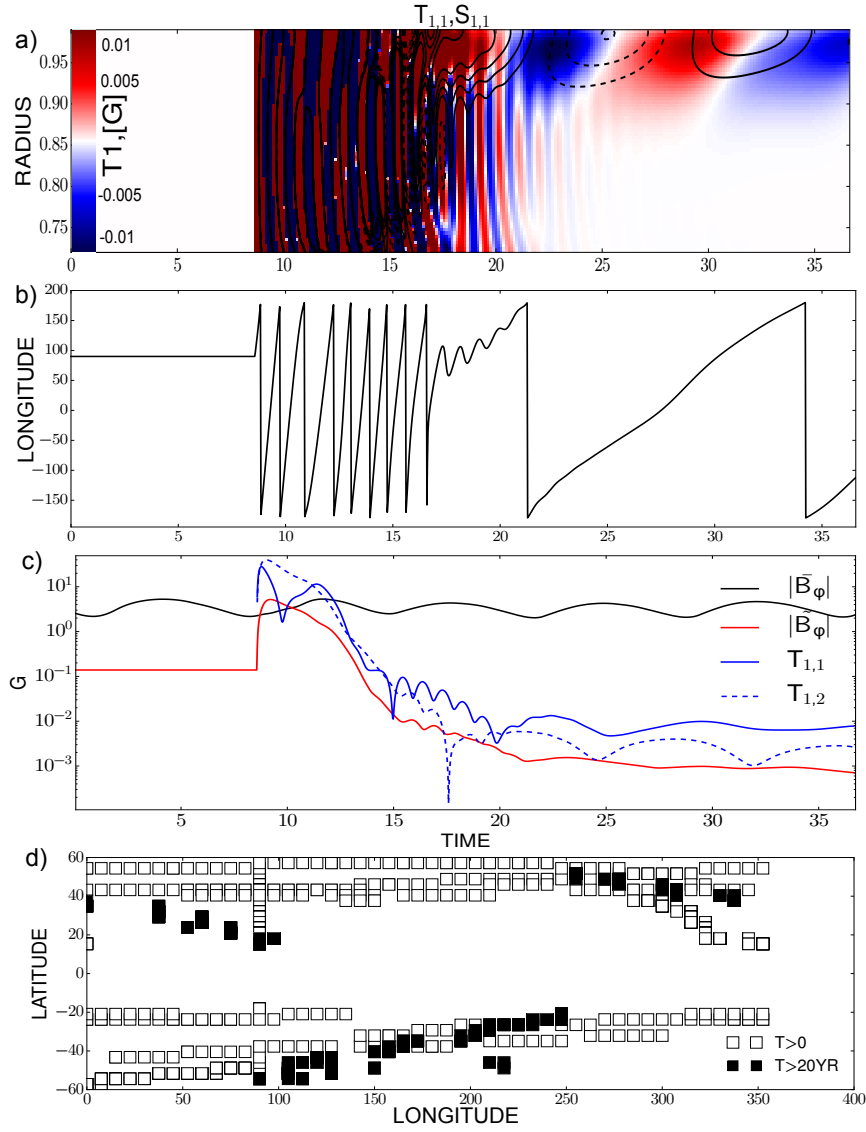


Fig. 6.— The same as Figure 5 for the model M2

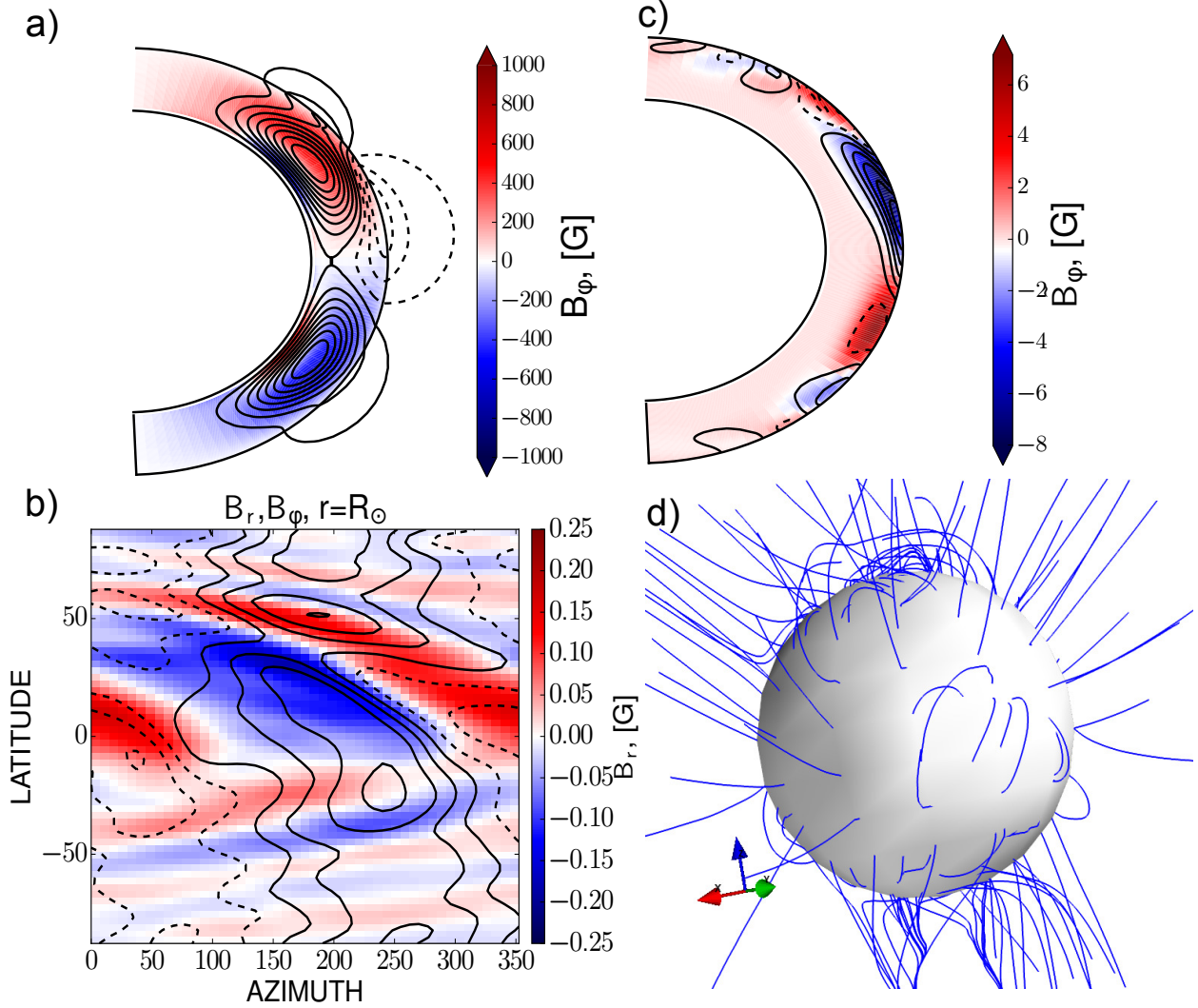


Fig. 7.— Model M1 half year after initialization of the non-axisymmetric perturbation, a) distribution of the axisymmetric toroidal magnetic field (background image) and poloidal field lines in the meridional cross-section, b) azimuth-latitude distribution of the large-scale radial magnetic field (background image) and toroidal magnetic field (contours are in the same range as for  $B_r$ ) on the surface; c) the same as a) for the non-axisymmetric components of magnetic field; d) the magnetic field lines above the surface.

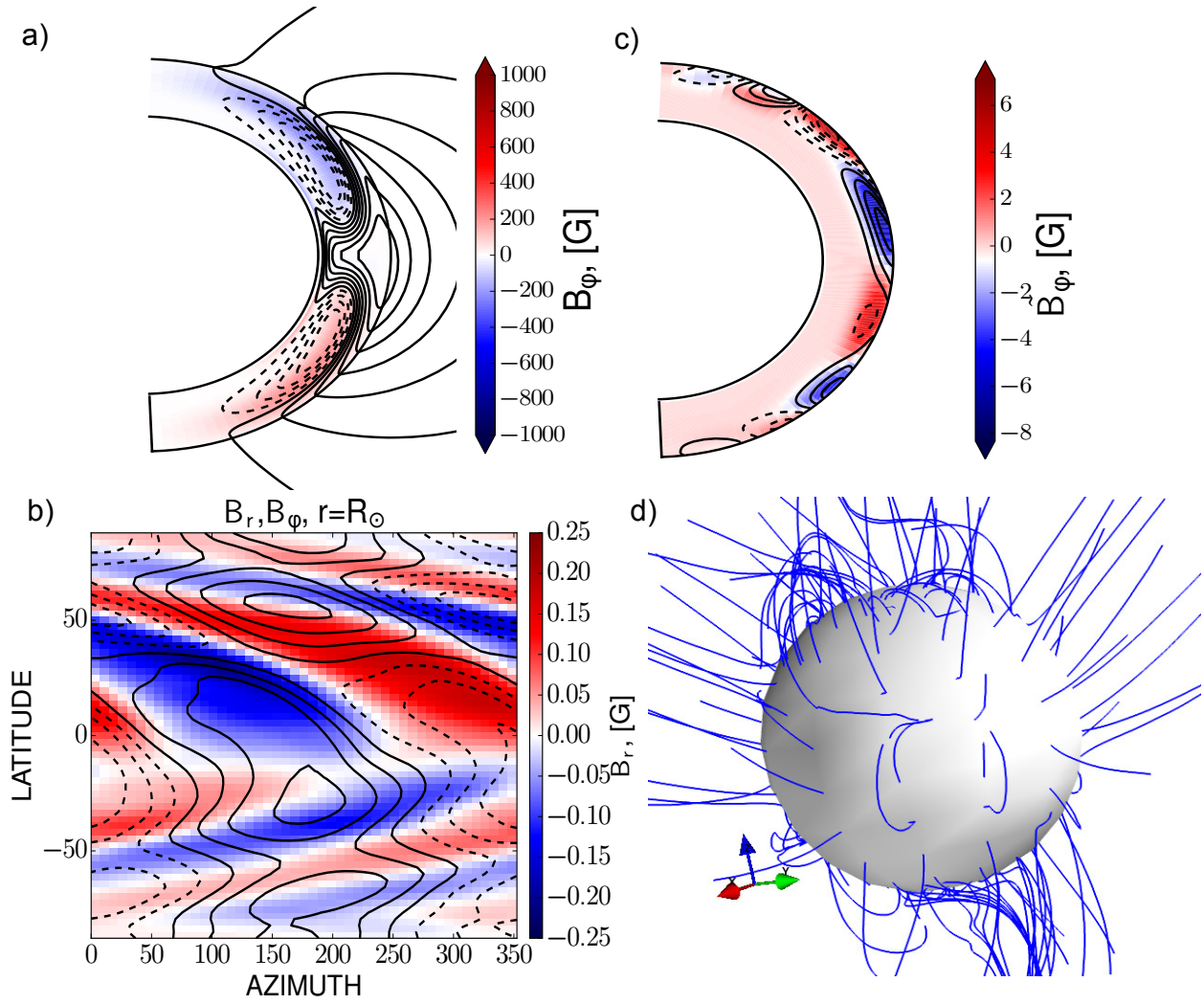


Fig. 8.— The same as Figure 7 for the model M2

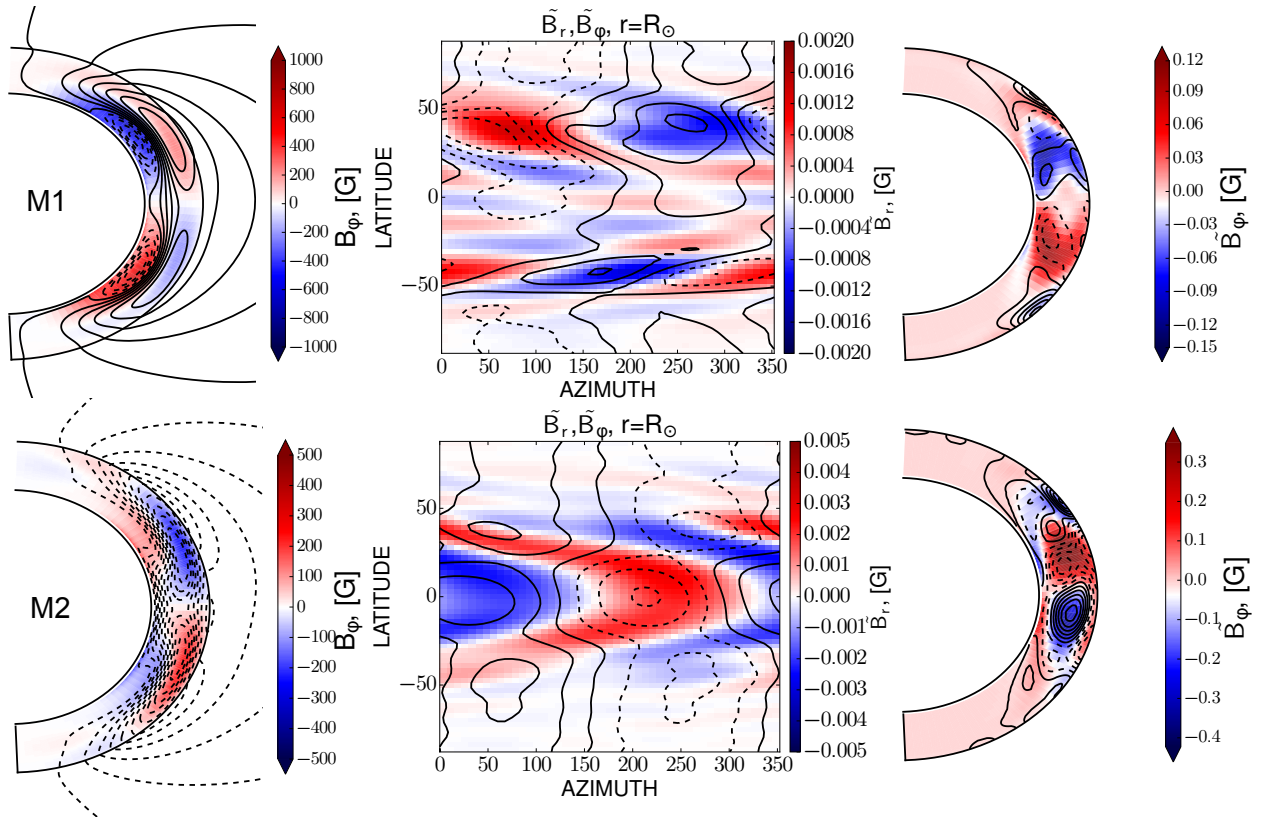


Fig. 9.— The same as Fig7 after 5 year evolution

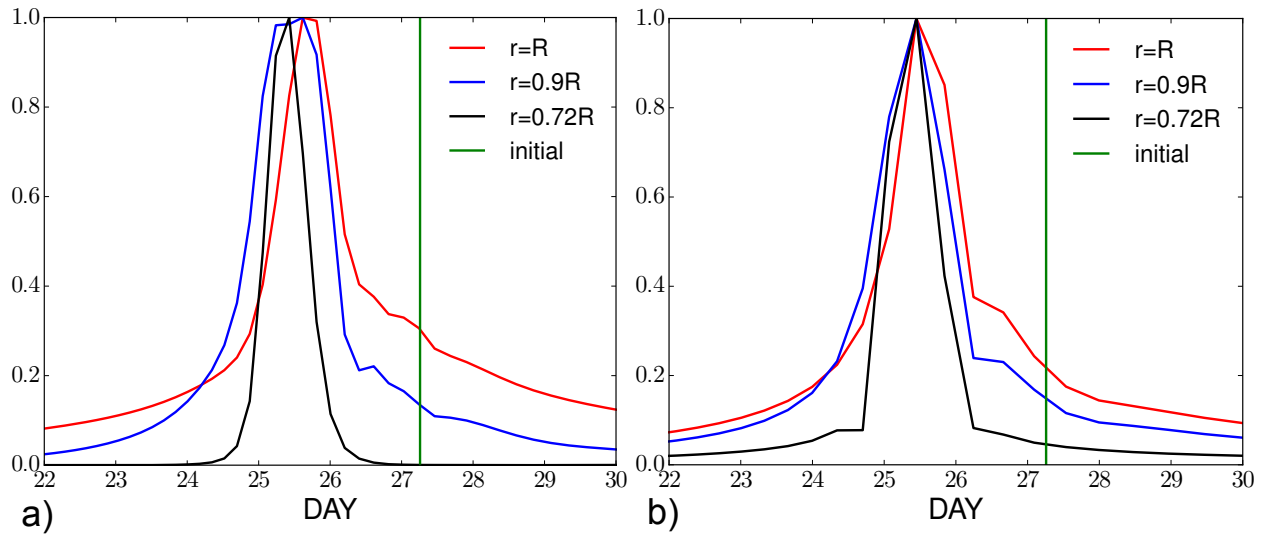


Fig. 10.— a) The model M0. The normalized power spectra for rotation periods of  $S_1$  at the three levels in the solar convection zone; b) the same as a) for the model M1

## REFERENCES

- Abramenko, V. I., Carbone, V., Yurchyshyn, V., Goode, P. R., Stein, R. F., Lepreti, F., Capparelli, V., & Vecchio, A. 2011, *ApJ*, 743, 133
- Berdyugina, S. V. 2004, *Sol. Phys.*, 224, 123
- Berdyugina, S. V., Moss, D., Sokoloff, D., & Usoskin, I. G. 2006, *A&A*, 445, 703
- Bigazzi, A., & Ruzmaikin, A. 2004a, *ApJ*, 604, 944
- . 2004b, *ApJ*, 604, 944
- Blackman, E. G., & Field, G. B. 2002, *Phys. Rev. Lett.*, 89
- Brandenburg, A., & Käpylä, P. J. 2007, *New Journal of Physics*, 9, 305
- Brandenburg, A., Rädler, K.-H., & Kemel, K. 2012, *A&A*, 539, A35
- Brandenburg, A., & Subramanian, K. 2005, *Phys. Rep.*, 417, 1
- Brown, B. P., Browning, M. K., Brun, A. S., Miesch, M. S., & Toomre, J. 2011, in *Astronomical Society of the Pacific Conference Series*, Vol. 448, 16th Cambridge Workshop on Cool Stars, Stellar Systems, and the Sun, ed. C. Johns-Krull, M. K. Browning, & A. A. West, 277
- Dikpati, M., & Gilman, P. A. 2001, *ApJ*, 559, 428
- Duvall, Jr., T. L., Scherrer, P. H., Svalgaard, L., & Wilcox, J. M. 1979, *Sol. Phys.*, 61, 233
- Elstner, D., & Korhonen, H. 2005, *Astronomische Nachrichten*, 326, 278
- Frisch, U., Pouquet, A., Léorat, J., & A., M. 1975, *J. Fluid Mech.*, 68, 769

- Gyenge, N., Baranyi, T., & Ludmány, A. 2012, *Central European Astrophysical Bulletin*, 36, 9
- Hoeksema, J. T. 1995, *Space Sci. Rev.*, 72, 137
- Howe, R., Larson, T. P., Schou, J., Hill, F., Komm, R., Christensen-Dalsgaard, J., & Thompson, M. J. 2011, *Journal of Physics Conference Series*, 271, 012061
- Hubbard, A., & Brandenburg, A. 2012, *ApJ*, 748, 51
- Käpylä, P. J., Mantere, M. J., & Brandenburg, A. 2012, *ApJ*, 755, L22
- Kichatinov, L. L. 1991, *Astron. Astrophys.*, 243, 483
- Kichatinov, L. L., & Pipin, V. V. 1993, *A&A*, 274, 647
- Kleeorin, N., & Rogachevskii, I. 2003, *Phys. Rev. E*, 67, 026321
- Kleeorin, N. I., & Ruzmaikin, A. A. 1982, *Magnetohydrodynamics*, 18, 116
- Krause, F., & Rädler, K.-H. 1980, *Mean-Field Magnetohydrodynamics and Dynamo Theory* (Berlin: Akademie-Verlag), 271
- Krivodubskij, V. N. 1987, *Soviet Astronomy Letters*, 13, 338
- Kuzanyan, K. M., Pipin, V. V., & Seehafer, N. 2006, *Sol.Phys.*, 233, 185
- Mitra, D., Candelaresi, S., Chatterjee, P., Tavakol, R., & Brandenburg, A. 2010, *Astronomische Nachrichten*, 331, 130
- Moffatt, H. K. 1978, *Magnetic Field Generation in Electrically Conducting Fluids* (Cambridge, England: Cambridge University Press)
- Moss, D. 1999, *MNRAS*, 306, 300

—. 2004, MNRAS, 352, L17

Moss, D., Tuominen, I., & Brandenburg, A. 1991, A&A, 245, 129

Muciaccia, P. F., Natoli, P., & Vittorio, N. 1997, ApJ, 488, L63

Parker, E. N. 1979, *Cosmical magnetic fields: Their origin and their activity* (Oxford: Clarendon Press)

Pipin, V. V. 2008, *Geophysical and Astrophysical Fluid Dynamics*, 102, 21

Pipin, V. V., & Kosovichev, A. G. 2011, ApJL, 727, L45

Pipin, V. V., & Kosovichev, A. G. 2013, *The Astrophysical Journal*, 776, 36

Pipin, V. V., & Kosovichev, A. G. 2014, ApJ, 785, 49

Pipin, V. V., Sokoloff, D. D., & Usoskin, I. G. 2012, A&A, 542, A26

Pipin, V. V., Zhang, H., Sokoloff, D. D., Kuzanyan, K. M., & Gao, Y. 2013, MNRAS, 435, 2581

Pouquet, A., Frisch, U., & Léorat, J. 1975, *J. Fluid Mech.*, 68, 769

Rädler, K.-H. 1969, *Monats. Dt. Akad. Wiss.*, 11, 194

Rädler, K.-H., Kleorin, N., & Rogachevskii, I. 2003, *Geophys. Astrophys. Fluid Dyn.*, 97, 249

Raedler, K.-H. 1986, *Astronomische Nachrichten*, 307, 89

Raedler, K.-H., Wiedemann, E., Brandenburg, A., Meinel, R., & Tuominen, I. 1990, A&A, 239, 413

Rogachevskii, I., Kleeorin, N., Käpylä, P. J., & Brandenburg, A. 2011, *Phys. Rev. E*, 84, 056314

Schrinner, M. 2011, *A&A*, 533, A108

Simard, C., Charbonneau, P., & Bouchat, A. 2013, *ApJ*, 768, 16

Stix, M. 2002, *The sun: an introduction*, 2nd edn. (Berlin : Springer), 521

Tuominen, I., Berdyugina, S. V., & Korpi, M. J. 2002, *Astronomische Nachrichten*, 323, 367

Tworowski, A., Covas, E., Tavakol, R., & Brandenburg, A. 1998, *ArXiv Astrophysics e-prints*

Zhao, J., Bogart, R. S., Kosovichev, A. G., Duvall, Jr., T. L., & Hartlep, T. 2013, *ApJ*, 774, L29

## 5. Appendix A

### 5.1. The $\mathcal{E}$

This section of Appendix describe some parts of the mean-electromotive force. We employ the anisotropic diffusion tensor which is derived by Pipin (2008) (hereafter P08) and Pipin & Kosovichev (2014):

$$\begin{aligned} \eta_{ijk} = & 3\eta_T \left\{ \left( 2f_1^{(a)} - f_2^{(d)} \right) \varepsilon_{ijk} + 2f_1^{(a)} e_i e_n \varepsilon_{jnk} \right. \\ & \left. + \frac{a}{3} \phi_1 (g_n g_j \varepsilon_{ink} - \varepsilon_{ijk}) \right\} + 3\eta_T C_\delta f_4^{(d)} e_j \left\{ \tilde{\varphi}_7^{(w)} \delta_{ik} + \tilde{\varphi}_2^{(w)} \frac{\overline{B_i B_k}}{\overline{B^2}} \right\}, \end{aligned} \quad (\text{A1})$$

where  $\mathbf{e} = \mathbf{\Omega}/\Omega$  is the unit vector along the rotation axis and  $\mathbf{g}$  is the unit vector in the radial direction,  $a$  is the parameter of the turbulence anisotropy,  $\eta_T$  is the magnetic diffusion coefficient. The diffusivity coefficients depend on the Coriolis number  $\Omega^* = 4\pi \frac{\tau_c}{P_{rot}}$ , where  $P_{rot}$  is the rotational period,  $\tau_c$  is the convective turnover time. The quenching functions  $f_{1,2}^{(a,d)}$  and  $\phi_1$  are

$$\begin{aligned} f_1^{(a)} &= \frac{1}{4\Omega^{*2}} \left( (\Omega^{*2} + 3) \frac{\arctan \Omega^*}{\Omega^*} - 3 \right), \\ f_2^{(d)} &= \frac{1}{\Omega^{*2}} \left( \frac{\arctan \Omega^*}{\Omega^*} - 1 \right), \\ \phi_1 &= -\frac{1}{24\Omega^{*2}} (2 \log(1 + 4\Omega^{*2}) + 4 \log(1 + \Omega^{*2}) \\ &\quad + (1 - 4\Omega^{*2}) \frac{\arctan(2\Omega^*)}{\Omega^*} + 4(1 - \Omega^{*2}) \frac{\arctan(\Omega^*)}{\Omega^*} - 6). \end{aligned}$$

The last term in the Eq.(A1) is a contribution of the  $\mathbf{\Omega} \times \mathbf{J}$  effect with a free parameter  $C_\delta$  and the quenching functions of the magnetic field and the Coriolis number,  $\tilde{\varphi}_{2,7}^{(w)}(\beta)$  and  $f_4^{(d)}(\Omega^*)$ :

$$\tilde{\varphi}_2^{(w)} = -\frac{5}{192\beta^5} \left( 3(16\beta^4 - 5) \frac{\arctan(2\beta)}{2\beta} - 5(4\beta^2 - 3) \right), \quad (\text{A2})$$

$$\tilde{\varphi}_7^{(w)} = \frac{5}{192\beta^4} \left( 3(16\beta^4 - 1) \frac{\arctan(2\beta)}{2\beta} - (4\beta^2 - 3) \right), \quad (\text{A3})$$

$$f_4^{(d)} = \frac{1}{6\Omega^{*3}} \left( (2\Omega^{*2} + 3) - 3(\Omega^{*2} + 1) \frac{\arctan(\Omega^*)}{\Omega^*} \right). \quad (\text{A4})$$

Note in the notation of P08  $\tilde{\varphi}_{2,7}^{(w)}(\beta) = \frac{5}{2}\varphi_{2,7}^{(w)}(\beta)$  and  $\beta = \frac{|\overline{B}|}{\sqrt{4\pi\bar{\rho}u^2}}$ .

The  $\alpha$  effect takes into account the kinetic and magnetic helicities,

$$\alpha_{ij} = C_\alpha \sin^2 \theta \psi_\alpha(\beta) \alpha_{ij}^{(H)} \eta_T + \alpha_{ij}^{(M)} \frac{\bar{\chi} \tau_c}{4\pi \bar{\rho} \ell^2} \quad (\text{A5})$$

where  $C_\alpha$  is a free parameter, the  $\alpha_{ij}^{(H)}$  and  $\alpha_{ij}^{(M)}$  express the kinetic and magnetic helicity parts of the  $\alpha$ -effect, respectively,  $\bar{\chi}$ - is the small-scale magnetic helicity and  $\ell$  is the typical

length scale of the turbulence. The  $\alpha_{ij}^{(H)}$  reads,

$$\begin{aligned} \alpha_{ij}^{(H)} &= \delta_{ij} \left\{ 3 \left( f_{10}^{(a)} \left( \mathbf{e} \cdot \boldsymbol{\Lambda}^{(\rho)} \right) + f_{11}^{(a)} \left( \mathbf{e} \cdot \boldsymbol{\Lambda}^{(u)} \right) \right) \right\} + \\ &+ e_i e_j \left\{ 3 \left( f_5^{(a)} \left( \mathbf{e} \cdot \boldsymbol{\Lambda}^{(\rho)} \right) + f_4^{(a)} \left( \mathbf{e} \cdot \boldsymbol{\Lambda}^{(u)} \right) \right) \right\} \\ &+ 3 \left\{ \left( e_i \Lambda_j^{(\rho)} + e_j \Lambda_i^{(\rho)} \right) f_6^{(a)} + \left( e_i \Lambda_j^{(u)} + e_j \Lambda_i^{(u)} \right) f_8^{(a)} \right\}. \end{aligned} \quad (\text{A6})$$

and the  $\alpha_{ij}^{(M)}$  reads:

$$\alpha_{ij}^{(M)} = 2f_2^{(a)} \delta_{ij} - 2f_1^{(a)} e_i e_j, \quad (\text{A7})$$

Below we give the functions of the Coriolis number defining the dependence of the  $\alpha$ -effect on the Coriolis number:

$$f_2^{(a)} = \frac{1}{4\Omega^{*2}} \left( (\Omega^{*2} + 1) \frac{\arctan \Omega^*}{\Omega^*} - 1 \right), \quad (\text{A8})$$

$$f_3^{(a)} = \frac{1}{4\Omega^{*2}} \left( 2 - 2 \frac{\arctan \Omega^*}{\Omega^*} \right), \quad (\text{A9})$$

$$f_4^{(a)} = \frac{1}{6\Omega^{*3}} \left( 3 (\Omega^{*4} + 6\Omega^{*2} + 5) \frac{\arctan \Omega^*}{\Omega^*} - (13\Omega^{*2} + 15) \right), \quad (\text{A10})$$

$$f_5^{(a)} = \frac{1}{\Omega^*} \left( (\Omega^{*2} + 3) \frac{\arctan \Omega^*}{\Omega^*} - 3 \right), \quad (\text{A11})$$

$$f_6^{(a)} = \frac{1}{6\Omega^{*3}} \left( 3 (\Omega^{*2} + 2) \frac{\arctan \Omega^*}{\Omega^*} - (\Omega^{*2} + 6) \right), \quad (\text{A12})$$

$$\begin{aligned} f_8^{(a)} &= -\frac{1}{12\Omega^{*3}} \left( 3 (4\Omega^{*2} + 2) \frac{\arctan \Omega^*}{\Omega^*} \right. \\ &\quad \left. - (10\Omega^{*2} + 6) \right), \end{aligned} \quad (\text{A13})$$

$$f_{10}^{(a)} = \frac{1}{\Omega^*} \left( 1 - (\Omega^{*2} + 1) \frac{\arctan \Omega^*}{\Omega^*} \right), \quad (\text{A14})$$

$$f_{11}^{(a)} = -\frac{1}{6\Omega^{*3}} \left( 3 (\Omega^{*2} + 1)^2 \frac{\arctan \Omega^*}{\Omega^*} - (5\Omega^{*2} + 3) \right), \quad (\text{A15})$$

The functions (27-36) were defined in P08 for the general case which includes the effects the hydrodynamic and magnetic fluctuations in the background turbulence. Here, we bring the expressions for the case when the background turbulent fluctuations of the small-scale magnetic field are in the equipartition with the hydrodynamic fluctuations, i.e.,

$\varepsilon = \frac{b'^2}{4\pi\bar{\rho}u'^2} = 1$ , where the  $u'^2$  and  $b'^2$  are intensity of the background turbulent velocity and magnetic field. The magnetic quenching function of the hydrodynamical part of  $\alpha$ -effect is defined by

$$\psi_\alpha = \frac{5}{128\beta^4} \left( 16\beta^2 - 3 - 3(4\beta^2 - 1) \frac{\arctan(2\beta)}{2\beta} \right). \quad (\text{A16})$$

Note in the notation of P08  $\psi_\alpha = -3/4\phi_6^{(a)}$ .

The turbulent pumping of the mean-field contains the sum of the contributions due to the mean density gradient (Kichatinov 1991),  $\gamma_{ij}^{(\rho)}$ , the diamagnetic pumping (Krivodubskij 1987),  $\gamma_{ij}^{(\eta)}$ , the mean-field magnetic buoyancy (Kichatinov & Pipin 1993),  $\gamma_{ij}^{(b)}$ , and due to effects of the large-scale shear (Rogachevskii et al. 2011),  $\gamma_{ij}^{(H)}$ :

$$\gamma_{ij} = \gamma_{ij}^{(\rho)} + \gamma_{ij}^{(\eta)} + \gamma_{ij}^{(b)} + \gamma_{ij}^{(H)}, \quad (\text{A17})$$

where each contribution is defined as follows:

$$\begin{aligned} \gamma_{ij}^{(\rho)} &= 3\eta_T \left\{ f_3^{(a)} \Lambda_n^{(\rho)} + f_1^{(a)} (\mathbf{e} \cdot \mathbf{\Lambda}^{(\rho)}) e_n \right\} \varepsilon_{inj} \\ &\quad - 3\eta_T f_1^{(a)} e_j \varepsilon_{inm} e_n \Lambda_m^{(\rho)} \end{aligned} \quad (\text{A18})$$

$$\gamma_{ij}^{(\eta)} = \frac{3}{2} C_v \eta_T \left\{ f_2^{(a)} \Lambda_n^{(\eta)} \varepsilon_{inj} + f_1^{(a)} e_j \varepsilon_{inm} e_n \Lambda_m^{(\eta)} \varepsilon_{inm} \right\} \quad (\text{A19})$$

$$\gamma_{ij}^{(b)} = \frac{\alpha_{MLT} u'}{\gamma} \beta^2 K(\beta) g_n \varepsilon_{inj}, \quad (\text{A20})$$

$$\gamma_{ij}^{(H)} = \left( f_2^{(\gamma)} \frac{\bar{\chi}}{\bar{\rho} \ell^2} + f_1^{(\gamma)} h_K \right) \tau_c^2 \varepsilon_{ikj} \bar{W}_k \quad (\text{A21})$$

where  $f_{1,2,3}^{(a)}(\Omega^*)$  and  $f_{1,2}^{(\gamma)}(\Omega^*)$  - are functions of the Coriolis number,  $u'$  is the RMS of the convective velocity,  $\Lambda_i^{(\rho)} = \nabla_i \log \bar{\rho}$  are components of the gradient of the mean density,  $\Lambda_i^{(\eta)} = \nabla_i \log \eta_T$  is the same for the turbulent diffusivity, the free parameter  $C_v$  is used to tune the BL-types models. In the D-type models we put  $C_v = 1$ . The  $\alpha_{MLT}$  is the parameter of the mixing length theory,  $\gamma$  is the adiabatic exponent,  $C_\beta$  is a free parameter

to switch on/off the effect in the model and  $\mathbf{g}$  is the unit vector in the radial direction. The quenching of the magnetic buoyancy (see (Kichatinov & Pipin 1993)) is determined by

$$K = \frac{1}{16\beta^4} \left( \frac{(\beta^2 - 3)}{\beta} \arctan(\beta) + \frac{(\beta^2 + 3)}{(\beta^2 + 1)} \right).$$

The pumping effect  $\gamma_{ij}^{(H)}$  is determined by the helicity parameters including the magnetic,  $\bar{\chi}$ , and kinetic helicity,  $h_{\mathcal{K}} = \frac{3\eta_T}{2\tau_c} F_1(\Omega^*) \cos\theta \frac{\partial}{\partial r} \log(\bar{\rho}u')$  (see, Kuzanyan et al. 2006), and the large-scale vorticity vector  $\overline{\mathbf{W}} = \nabla \times \overline{\mathbf{U}}$ . Dependence of the  $\gamma_{ij}^{(H)}$  on the Coriolis number is controlled by the quenching functions:

$$f_1^{(\gamma)} = \frac{1}{(24\Omega^*)^2} \left( (1300\Omega^{*2} + 391) \frac{\arctan(2\Omega^*)}{2\Omega^*} - 1456(\Omega^{*2} + 1) \frac{\arctan(\Omega^*)}{\Omega^*} - 3(32\Omega^{*2} - 355) \right), \quad (\text{A22})$$

$$F_1 = \frac{1}{2\Omega^*} \left( (\Omega^{*2} - 1) \frac{\arctan \Omega^*}{\Omega^*} + 1 \right) \quad (\text{A23})$$

and  $f_2^{(\gamma)} = 3f_2^{(a)}$ .